International Research Journal of Multidisciplinary Scope (IRJMS), 2025; 6(1):1225-1238 IRJMS

Original Article | ISSN (O): 2582-631X DOI: 10.47857/irjms.2025.v06i01.02815

Influence of Hall Effect and Radiation on Melting Heat Transfer of Magnetohydrodynamic Hybrid Nanofluid Flow over a Sheet with Variable Thickness

Narmatha M[1], Sumathi K[2]*, Panneer Selvi R[2]

[1]Department of Mathematics, KPR Institute of Engineering and Technology, Coimbatore, India, [2]Department of Mathematics, PSGR Krishnammal College for Women, Coimbatore, India. *Corresponding Author's Email: sumathiarunmath@gmail.com

Abstract

The focus of this work is to analyses the radiation and Hall current effect in a hybrid nanofluid with melting heat transfer flowing magneto hydrodynamically across a variable thickness sheet. The mathematical formulation involves a system of partial differential equations (PDEs), which are transformed into Ordinary differential equations (ODEs) through the application of suitable similarity transformation. The MATLAB (9.14) software's bvp4c approach (Shooting method) performs the numerical calculations. This study highlights the influence of Hall Effect, melting heat rate, and MHD on several flow parameters, such as temperature, fluid velocity, skin friction and Nusselt number distributions. The results are displayed graphically. Hybrid nanofluid and Hall Effect drastically change the flow and temperature properties.

Keywords: Hall Effects, Melting Heat, MHD, (SWCNTs +C_8H_{18}) - Nanofluid, (SWCNTs + Ag + C_8H_{18}) - Hybrid Nanofluid, Variable Thickness Sheet.

Introduction

Heat transfer in nanofluids has attracted a lot of interest because of its enhanced thermal characteristics over conventional fluids and hybrid nanofluids, which comprise two or more types of nanoparticles. Initially, Choi and Eastman (1) revealed that thermal conductivity improved when nanoparticles were floating in the fluids. The heat transfer effect from the sheet to the fluid was examined by Vajravelu (2). A non-flatness surface significantly affects the boundary layer's formation and results in mass suction when the index power velocity is less than one and the mass injection effect when the index power value is greater than one (3). Anjali Devi and Prakash (4) explored the implications of radiative heat transfer on hydromagnetic flow on a thin stretched sheet and explored the complex interaction between thermal and magnetic characteristics in fluid motion. Some researchers present a thorough analysis of current and future industrial uses of carbon nanotubes, emphasizing how their distinct electrical, mechanical and thermal properties have the potential to revolutionize a number of industries (5). Researchers in the past (6) used homotopy analysis and similarity transformations to delve into the mass and heat transport of a nanofluid across a stretched sheet with varying thicknesses. In the past researcher (7) explored the significance of several characteristics on the fluid in a velocity and temperature profile, highlighting the part fractional derivatives and weight coefficients play in determining boundary layer thickness. A mathematical model that depicts the progressive melting of ice on a flat surface was created by Roberts (8). In order to acquire numerical findings examined (9), the PDEs driving nonlinear motion in the nanofluid model are converted into ODEs while accounting for the effects of thermophoresis and Brownian motion. Important findings about melting heat transfer are also found in the past research (10–12) for a variety of models, including nanofluids like carbon nanotubes, couple stress, and micropolar fluid with heat absorption, which illustrate how different parameters affect temperature and velocity distributions. Turkyilmazoglu examined the uneven flow of an oily nanofluid that conducts electricity via an endless vertical normal plate (13). Hydromagnetic boundary layer fluid flow past a stretching sheet was quantitatively investigated in this work, taking

(Received 12th October 2024; Accepted 27th January 2025; Published 31st January 2025)

into consideration the effects of a magnetic field, radiation and thermophoresis effect. Previous studies shown that how temperature, concentration, velocity, heat transfer rates, and skin friction are affected by additional significant parameters (14, 15). Hybrid nanofluid has a greater impact than nanofluid when exposed to radiation, heat generation, and other chemical reactions across a rotating stretched sheet (16). Some researchers examined heat transmission and magnetic parameters in a nanofluid across a thin, variable-thickness elastic sheet (17).

The impacts of heat radiation, mass diffusion, and magneto hydrodynamic flow of fluids along the particle across a stretching sheet (non linear) with varying thickness are covered in this work. While the electric field raises temperature and velocity, it lowers concentration (18, 19). A thicker boundary layer results from thermal radiation, which also causes a significant temperature increase. Previous findings addressed the Hall Effect on magnetohydrodynamic flow and heat transport of an electrically conducting fluid over a stretched sheet of variable thickness and used the FDM (finite difference method) to answer the problem (20). The impacts of Hall current, Cattaneo-Christov heat flux, and permeability that improve fluid performance and heat transport rate in real-world applications were the main topics of Parida*et al.* and Aamir Ali *et al.* (21, 22).

Other researchers evaluated the stagnation point flow of gasoline oil as base fluid, carbon nanotubes as nanoparticles and copper oxide as hybrid nanoparticles over a stretching sheet (23). The melting heat transfer flow around the stagnation point across a stretching sheet of different thickness was observed by others using carbon nanotubes (SWCNTs, MWCNTs) as a nanoparticle and water and kerosene as base fluids (24). Hybrid nanofluid flow over a stagnation point using a variable thickness sheet (25). The efficiency of high-temperature cooling applications, including solar energy, electrical equipment, and the automobile industry, was investigated by researchers with a primary focus on the combination of silver, titanium oxide, and water (26).

Hall current becomes prominent if the magnetic flux amplitude is very high or the low fluid density. It finds numerous applications in Hall devices, electrical circuits, pumps, inverters, turbines and more. The Hall Effect in hybrid nanofluid flow has recently attracted significant research attractions and it is clear from the earlier literature that the Hall Effect was not studied much more. But Hall current affects the flow of the fluid, the temperature, and the pressure gradient in case of hybrid nanofluids. Two or more types of nanoparticles suspended in a base fluid make up a hybrid nanofluid. Single walled carbon nanotubes (SWCNTs) suspended in gasoline (the base fluid) make up the nanofluid used in this work, whereas silver (Ag) nanoparticles and SWCNTs in gasoline (the base fluid) combine to form the hybrid nanofluid. This prompted the present study to concentrate Hall current effect on hybrid nanofluid across a variable thickness sheet. The shooting technique is used to solve the governing equations, and numerical and graphical analyses are performed to determine the effects of different flow parameters on temperature, skin friction, velocity, and Nusselt number. This issue is especially pertinent to situations involving nuclear reactors, solar energy systems, manufacturing processes, thermal management systems, aerospace engineering, and biomedical devices.

Formulation

Take into consideration a hybrid nanofluid flowing across a stretched sheet of varying thickness. Based on cartesian coordinates, the y-axis shown in Figure 1 is perpendicular to the stretching sheet, and the stretching velocity $U_W = U_0(x+b)^m$ causes the sheet to stretch in the x-axis's direction. The thickness of the sheet is taken as $y = b^*(x+b)^{\frac{1-m}{2}}$, indicating the sheet thickness along the x-axis. It is assumed that all the fluid properties remains constant. The thermal characteristics of nanoparticles are presented in Table 1.

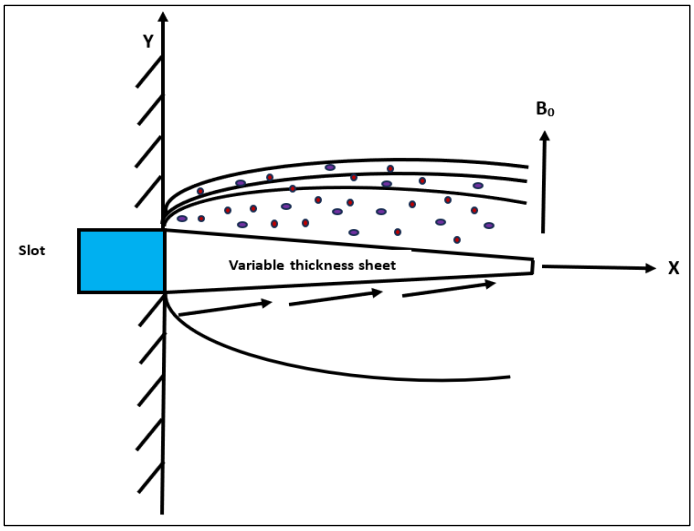

Figure 1: Diagrammatic Flow over a Variable Thickness Sheet

The governing equations, predicated on the assumptions above, are

$$\frac{\partial u}{\partial x}+\frac{\partial v}{\partial y}=0 \qquad [1]$$

$$u\frac{\partial u}{\partial x}+v\frac{\partial u}{\partial y}=U_e\frac{dU_e}{dx}+\upsilon_{hnf}\frac{\partial^2 u}{\partial y^2}-\frac{\sigma B_0^2}{\rho_{hnf}}\frac{1}{1+\lambda^2}(U-U_e) \qquad [2]$$

$$u\frac{\partial T}{\partial x}+v\frac{\partial T}{\partial y}=\alpha_{hnf}\frac{\partial^2 T}{\partial y^2}+\frac{\upsilon_{hnf}}{(\rho C_p)_{hnf}}\left(\frac{\partial u}{\partial y}\right)^2-\frac{\partial q_r}{\partial y} \qquad [3]$$

The following initial and boundary conditions are applied to [1] – [3]:

$$u=U_w(x)=U_0(x+b)^m, v=0, T=T_m \text{at } y=b^*(x+b)^{\frac{1-m}{2}}$$

$$u\to U_e(x)=U_\infty(x+b)^m, T\to T_\infty \text{ at } y\to\infty \qquad [4]$$

Conditions of melting heat are considered as

$$k_{hnf}\left(\frac{\partial T}{\partial y}\right)_{y=b^*(x+b)^{\frac{1-m}{2}}}=\rho_{hnf}[\beta+C_s(T_m-T_0)]v_{y=b^*(x+b)^{\frac{1-m}{2}}} \qquad [5]$$

Rosseland Approximation is used to make the problem mathematically tractable in radiative transport with an effective thermal conductivity. By Rosseland approximation heat flux can be expressed as

$$q_r=-\frac{4\sigma^*\partial T^4}{3k^*\partial y}=-\frac{16\sigma^*}{3k^*}T^3\frac{\partial T}{\partial y} \qquad [6]$$

Where k^* is mentioned as the coefficient of absorption, σ^* is mentioned as the Stefan-Boltzmann constant and T^4 is used to express the Taylor series up to T_∞ is

$$T^4=4T_\infty^3T-3T_\infty^4 \qquad [7]$$

Table 1: Thermal characteristics of nanoparticles (25)

Nanoparticle/Thermophysical properties	$\rho\left(\frac{kg}{m^3}\right)$	$k\left(\frac{W}{mK}\right)$	$C_p\left(\frac{J}{kgK}\right)$	**Pr**
SWCNTs	1600	3000	796	-
Ag	10490	235	429	-
Gasoline oil	750	0.114	425	9.4

We choose the transformations,

$$\eta=\sqrt{\frac{m+1}{2\upsilon_f}U_0(x+b)^{m-1}}.y,\ \psi=\sqrt{\frac{2\upsilon_f}{m+1}U_0(x+b)^{m+1}}f^*(\eta),\qquad \theta^*(\eta)=\frac{T-T_m}{T_\infty-T_m},$$

$$u=U_0(x+b)^m f^{*'}(\eta),\ \ v=-\sqrt{\frac{(m+1)\upsilon_f}{2}U_0(x+b)^{m-1}}\left(f^*(\eta)+\eta f^{*'}(\eta)\frac{m-1}{m+1}\right) \qquad [8]$$

Equations [1] through [3] are simplified by using the aforementioned similarity transformations.

$$\frac{A_{11}}{(1-\varphi_1)^{2.5}(1-\varphi_2)^{2.5}} f^{*'''} + f^* f^{*''} + \frac{2m}{m+1}(A^2 - f^{*'^2}) - \frac{Ha^2}{1+\lambda^2}\left(f^{*'} - A\right) = 0 \quad [9]$$

$$\left(\frac{k_{hnf}}{k_f} + \frac{4}{3}Rd\right)\theta^{*''} + \frac{PrPr\,Ec}{(1-\varphi_1)^{2.5}(1-\varphi_2)^{2.5}} f^{*''^2} + B_{11} Pr\theta^{*'} f^* = 0 \quad [10]$$

The modified boundary conditions are

$$f^{*'}(\alpha) = 1, \theta^*(\alpha) = 0, \frac{k_{hnf}}{k_f} M\theta^{*'}(\alpha) + A_{11}\left(Prf^*(\alpha) + \alpha\frac{m-1}{m+1}\right) = 0 \text{ at } \alpha = b^*\sqrt{\frac{m+1}{2\upsilon_f}U_0}$$

$$f^{*'}(\infty) \to A, \theta^*(\infty) \to 1 \text{ as } \alpha \to \infty \quad [11]$$

Where

$$A_{11} = \frac{1}{(1-\varphi_2)\left((1-\varphi_1)+\varphi_1\frac{\rho_{s1}}{\rho_f}\right)+\varphi_2\frac{\rho_{s2}}{\rho_f}} \quad [12]$$

$$B_{11} = \left((1-\varphi_2)\left((1-\varphi_1)C_{pf} + \varphi_1\frac{(\rho C_p)_{s2}}{\rho_f}\right)\right) + \varphi_2\frac{(\rho C_p)_{s1}}{\rho_f} \quad [13]$$

where prime denotes derivative for η and wall thickness is $\alpha = b^*\sqrt{\frac{m+1}{2\upsilon_f}U_0}$ which gives a flat surface. Here we define $f^*(\eta) = f(\eta - \alpha) = f(\xi)$.

Hence equations [9] and [10] become

$$\frac{A_{11}}{(1-\varphi_1)^{2.5}(1-\varphi_2)^{2.5}} f''' + ff'' + \frac{2m}{m+1}(A^2 - f'^2) - \frac{Ha^2}{1+\beta^2}(f' - A) = 0 \quad [14]$$

$$\left(\frac{k_{hnf}}{k_f} + \frac{4}{3}Rd\right)\theta'' + \frac{PrPr\,Ec}{(1-\varphi_1)^{2.5}(1-\varphi_2)^{2.5}} f''^2 + B_{11} Pr\theta' f = 0 \quad [15]$$

Boundary conditions are

$$f'(0) = 1, \theta(0) = 0, \frac{k_{hnf}}{k_f} M\theta'(0) + A_{11}\left(Prf(0) + \alpha\frac{m-1}{m+1}\right) = 0,$$

$$f'(\infty) \to A, \theta(\infty) \to 1 \text{ when } \xi \to \infty \quad [16]$$

The non-dimensional parameters involved are

$$A = \frac{U_\infty}{U_0}, \qquad \alpha = b^*\sqrt{\frac{m+1}{2\upsilon_f}U_0}, \qquad Pr = \frac{\mu C_p}{k}, Ec = \frac{U_0^2(x+b)^{2m}}{(T_\infty - T_m)C_{p_f}},$$

$$M = \frac{C_{p_f}(T_\infty - T_m)}{\lambda + C_s(T_m - T_0)}, Ha^2 = \frac{\sigma B_0^2 (x+b)^{m-1}}{\rho_f U_0}, Rd = \frac{4\sigma T^3}{kk_f} \quad [17]$$

Expression for Wall Friction Coefficient and Heat Transfer - Local Nusselt Number

Wall friction coefficient(C_f) is defined as $C_f = \frac{\tau_w}{\rho_f U_w^2}$ [18]

where $\tau_w = \mu_{hnf}\left(\frac{\partial u}{\partial y}\right)_{y=b^*\sqrt{\frac{m+1}{2\upsilon_f}U_0}}$ [19]

Local Nusselt number(Nu_x) is defined as $Nu_x = \frac{(x+b)q_w}{k(T_\infty - T_m)}$ [20]

where $q_w = -k_{hnf}\left(\frac{\partial T}{\partial y}\right)_{y=b^*\sqrt{\frac{m+1}{2\upsilon_f}U_0}}$ [21]

Substitute equations [8], [19] and [21] in equations [18] and [20] we get,

$$C_f\sqrt{Re_x} = \frac{1}{(1-\varphi_1)^{2.5}(1-\varphi_2)^{2.5}}\sqrt{\frac{m+1}{2}} f''(0) \quad [22]$$

$$\frac{Nu_x}{\sqrt{Re_x}} = -\frac{k_{hnf}}{k_f}\sqrt{\frac{m+1}{2}}\theta'(0) \quad [23]$$

where local Reynolds number defined as $Re_x = \frac{U_0(x+b)^{m+1}}{\upsilon_f}$.

Table 2: The Model for Nanofluid and Hybrid Nanofluid Express about Density, Dynamic Viscosity, Kinematic Viscosity, Thermal Conductivity and Specific Heat Capacity

Nanofluid	Hybrid nanofluid
$\mu_{nf} = \frac{\mu_f}{(1-\varphi_1)^{2.5}}$	$\mu_{hnf} = \frac{\mu_f}{(1-\varphi_1)^{2.5}(1-\varphi_2)^{2.5}}$
$\upsilon_{nf} = \frac{\mu_{nf}}{\rho_{nf}}$	$\upsilon_{hnf} = \frac{\mu_{hnf}}{\rho_{hnf}}$
$(\rho C_p)_{nf} = (1-\varphi_1)(\rho C_p)_f + \varphi_1(\rho C_p)_{s1}$	$(\rho C_p)_{hnf} = (1-\varphi_2)\left((1-\varphi_1)(\rho C_p)_f + \varphi_1(\rho C_p)_{s1}\right) + \varphi_2(\rho C_p)_{s2}$
$\rho_{nf} = (1-\varphi_1)\rho_f + \varphi_1\rho_{s1}$	$\rho_{hnf} = (1-\varphi_2)\left((1-\varphi_1)\rho_f + \varphi_1\rho_{s1}\right) + \varphi_2\rho_{s2}$
$\frac{k_{nf}}{k_f} = \frac{k_{s1} + (n-1)k_f - (n-1)\varphi_1(k_f - k_{s1})}{k_{s1} + (n-1)k_f + \varphi_1(k_f - k_{s1})}$	$\frac{k_{hnf}}{k_f} = \frac{k_{s2} + (n-1)k_f - (n-1)\varphi_2(k_f - k_{s2})}{k_{s2} + (n-1)k_f + \varphi_2(k_f - k_{s2})}$
	$\frac{k_{bf}}{k_f} = \frac{k_{s1} + (n-1)k_f - (n-1)\varphi_1(k_f - k_{s1})}{k_{s1} + (n-1)k_f + \varphi_1(k_f - k_{s1})}$

Model for Nanofluid and Hybrid Nanofluid

For nanofluid and hybrid nanofluid we obtained the model presented in Table 2.

Methodology

To solve governed flow expressions (ODEs), the shooting approach(bvp4c) was created. Consequently, we follow the steps mentioned below.

$$h_1 = f$$
$$h_2 = h_1' = f'$$
$$h_3 = h_2' = f''$$
$$h_4 = h_3' = f''' =$$
$$-\frac{(1-\varphi_1)^{2.5}(1-\varphi_2)^{2.5}}{A_{11}}\left(h_1 h_3 + \frac{2m}{m+1}(A^2 - {h_2}^2) - \left(\frac{Ha^2}{1+\lambda^2}\right)(h_2 - A)\right)$$
$$h_6 = h_5' = \theta'' = \frac{1}{\left(\frac{k_{hnf}}{k_f} + \frac{4}{3}Rd\right)}\left(-B_{11}Pr h_1 h_6 - \frac{Pr\ Pr\ Ec}{(1-\varphi_1)^{2.5}(1-\varphi_2)^{2.5}}(h_3)^2\right)$$

$$h_2(0) = 1, h_5(0) = 0,$$
$$\frac{k_{hnf}}{k_f} M h_6(0) + A_{11}\left(Pr h_1(0) + \alpha\frac{m-1}{m+1}\right) = 0,$$
$$h_2(\infty) \to A, h_5(\infty) \to 1\ as\ \xi \to \infty.$$

Analysis

This study examines the effects on velocity, local Nusselt number, temperature, and skin friction coefficient. Furthermore, $\varphi_1 = \varphi_2 = 0.0$ for base fluid, $\varphi_2 = 0.0$ for nanofluid, and $\varphi_1$and $\varphi_2$are modified for hybrid nanofluid during a comparative analysis. A comparison between hybrid nanofluid and base fluid and nanofluid is conducted.

Results and Discussion

The shooting technique is used to numerically solve the system of ordinary differential equations [13] and [14] for temperature and velocity with the boundary conditions (15). The results are displayed graphically. Without the Hall Effect or magnetic parameter, Figure 2 illustrates the influence of the volume percentage of single-walled carbon nanotubes on the velocity distribution in comparison to a prior work by Muhammad *et al.* (25). There is a better agreement between the results and the previous study. The flow of $f'(\eta)$ against volume fraction φ_1 is shown in Figure 3. Velocity $f'(\eta)$ maximizes with an increments in φ_1 during the relative analysis of nanofluid is a combination of SWCNTs and Gasoline and hybrid nanofluid is a combination of Ag, SWCNTs and Gasoline. Additionally, a noticeable impact has been observed in hybrid nanofluid. Figure 4 discusses the flow of $f'(\eta)$ against the hybrid nanofluid's volume fraction, φ_2. The velocity $f'(\eta)$ was found to maximize as a result of the increase in the volume percentage of silver. Figures 5 and 6 illustrate how the magnetic parameter and flow index behavior (m<1) affect the velocity profile.

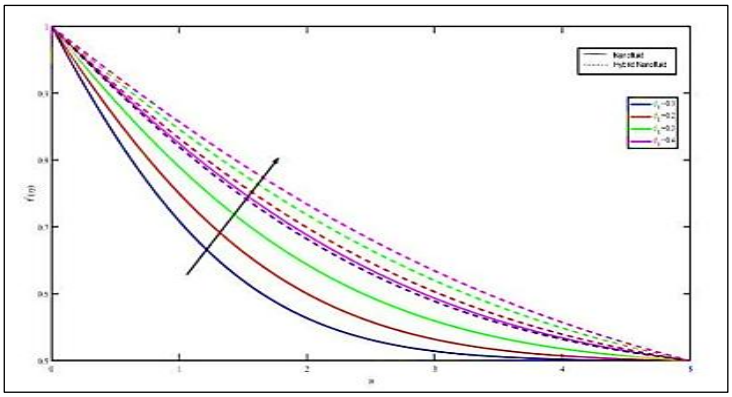

Figure 2: Influence of Volume Fraction φ_1 on $f'(\eta)$ at Ha =0, $\lambda = 0$

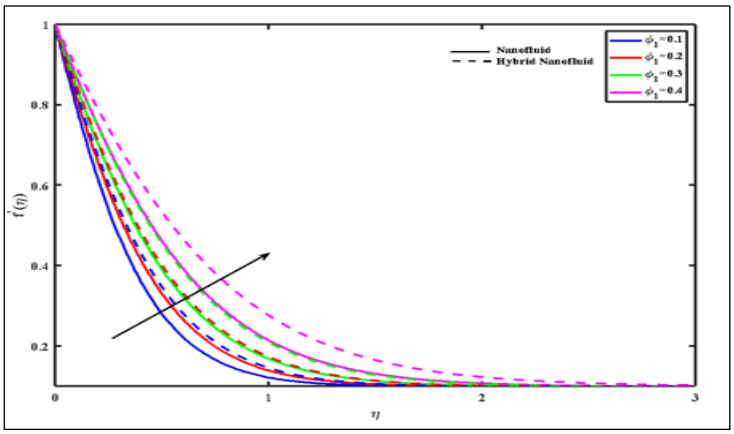

Figure 3: Influence of Volume Fraction (SWCNTs) φ_1 on $f'(\eta)$

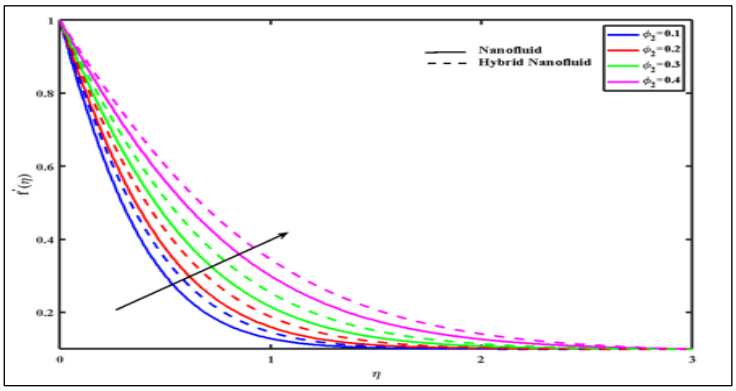

Figure 4: Influence of Volume Fraction (Silver) φ_2 on $f'(\eta)$

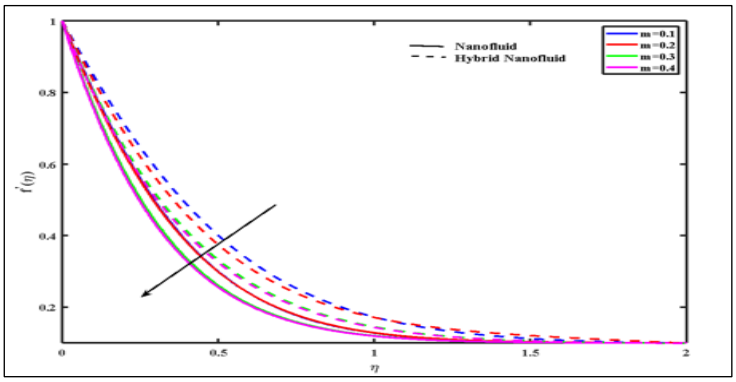

Figure 5: Influence of Index Behaviour m on $f'(\eta)$

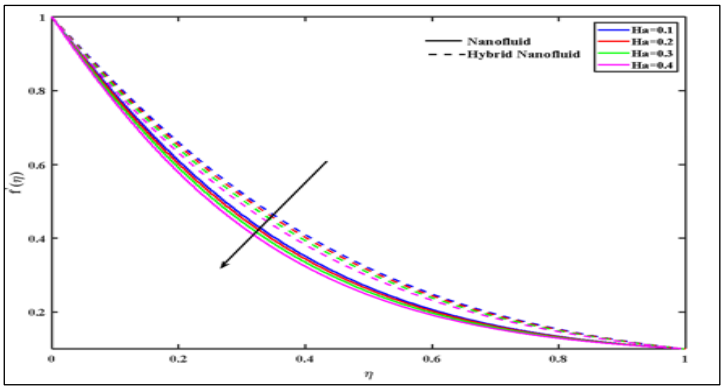

Figure 6: Influence of Magnetic Parameter Ha on $f'(\eta)$

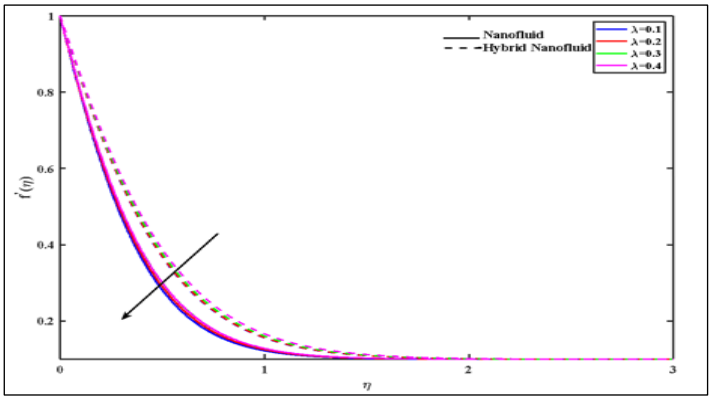

Figure 7: Influence of Hall Current λ on $f'(\eta)$

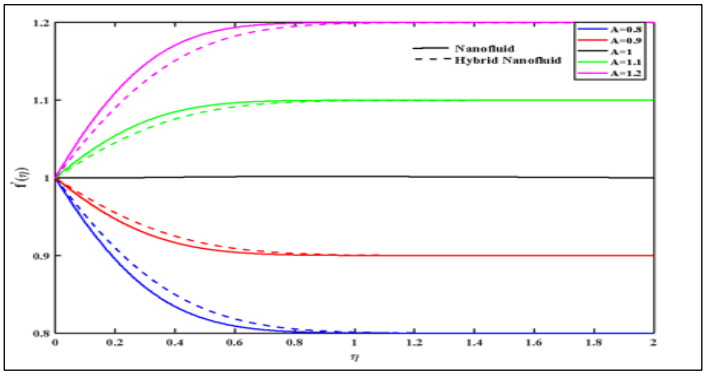

Figure 8: Influence of Velocity Ratio A on $f'(\eta)$

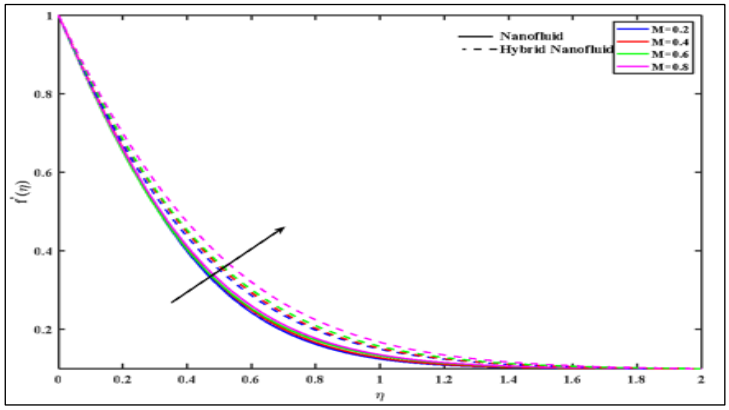

Figure 9: Influence of Melting Parameter M on $f'(\eta)$

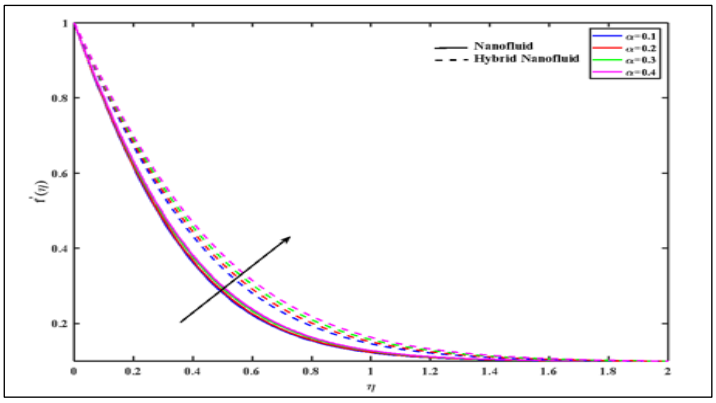

Figure 10: Influence of Wall Thickness α on $f'(\eta)$

The velocity profile has been observed to drop as the index behavior and magnetic parameter increase, and the impacts are particularly apparent in hybrid nanofluid. Figure 7 depicts the velocity profile as a function of λ. From the portray, it is clear that, the velocity is minimized due to the enhancement of Hall parameter. This is due to the fact that the effective conductivity $\frac{\sigma}{1+\lambda^2}$ decreases with increasing λ. For higher values of λ, the term $\frac{1}{1+\lambda^2}$ becomes very small and hence the resistive effect of the magnetic field diminishes. The effect of A on the velocity profile is shown in Figure 8. It is observed that the boundary layer will not exist when $A = 0$ whereas $A < 1$ indicates boundary layer thinning and $A > 1$ indicates boundary layer thickening.

The velocity profile in relation to the melting parameter (M) and wall thickness (α) is depicted in Figures 9 and 10. It was found that as M and α are increased, the velocity profile accelerates. Additionally, in each of the aforementioned instances, hybrid nanofluid has demonstrated a more noticeable effect than nanofluid.

With the relative analysis of nanofluid and hybrid nanofluids, Figures 11–18 show the temperature profile $\theta(\eta)$ as a function of the volume fraction of SWCNTs, volume of Ag, index behavior, Hall effect, wall thickness ratio, radiation parameter, magnetic parameter, and Eckert number.

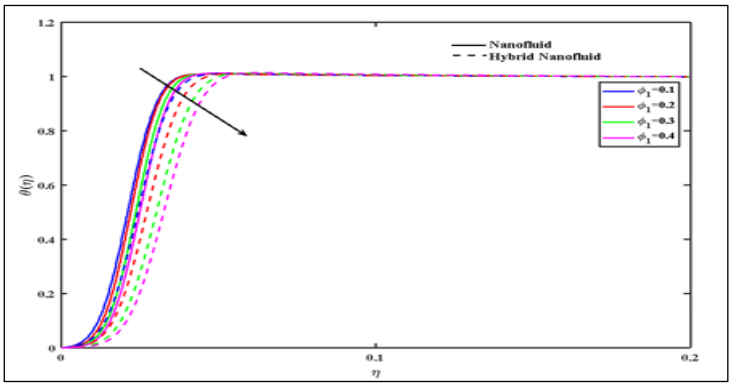

Figure 11: Influence of Volume Fraction φ_1 on $\theta(\eta)$

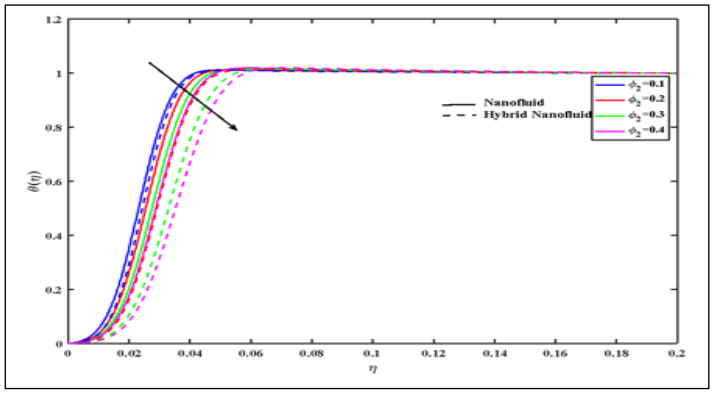

Figure 12: Influence of Volume Fraction φ_2 on $\theta(\eta)$

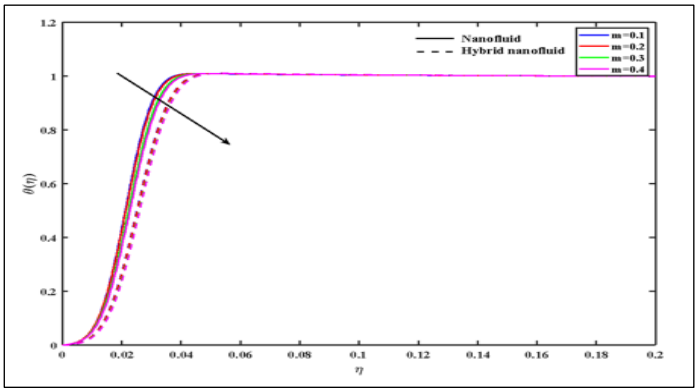

Figure 13: Influence of Index Behavior m on $\theta(\eta)$

Figure 11 shows the effect of volume fraction $\varphi_1$against $\theta(\eta)$. It was observed that the temperature profile is decreased when φ_1 is enhanced. Figure 12 shows the volume fraction of silver against $\theta(\eta)$. It is discovered that when φ_1 is enhanced, the temperature profile reduces. Figure 13 shows the index behavior on temperature curves.

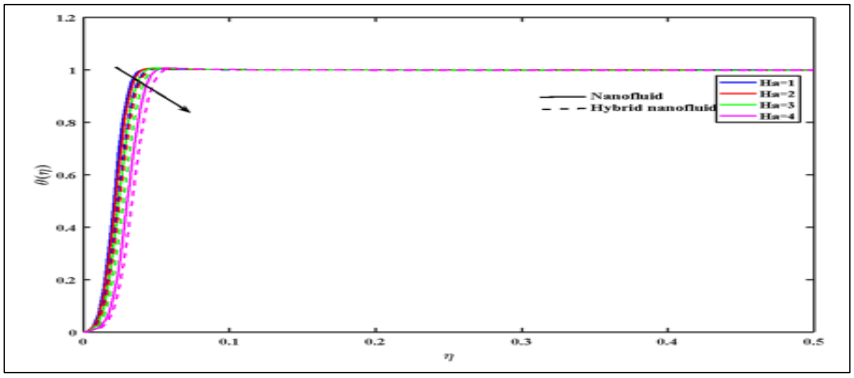

Figure 14: Influence of Magnetic Parameter Ha on $\theta(\eta)$

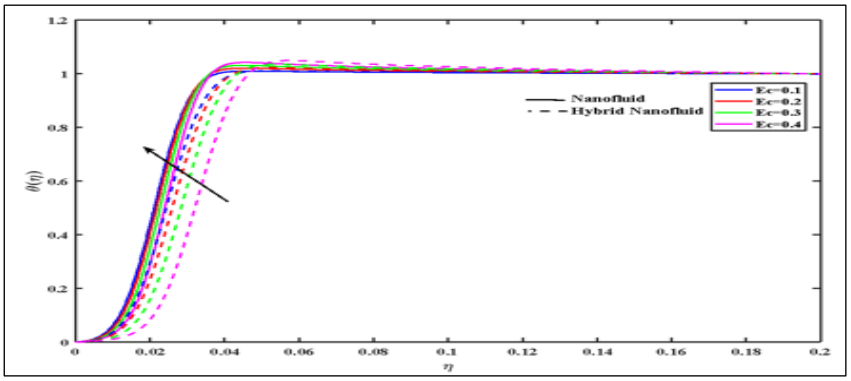

Figure 15: Influence of Eckert Number Ec on $\theta(\eta)$

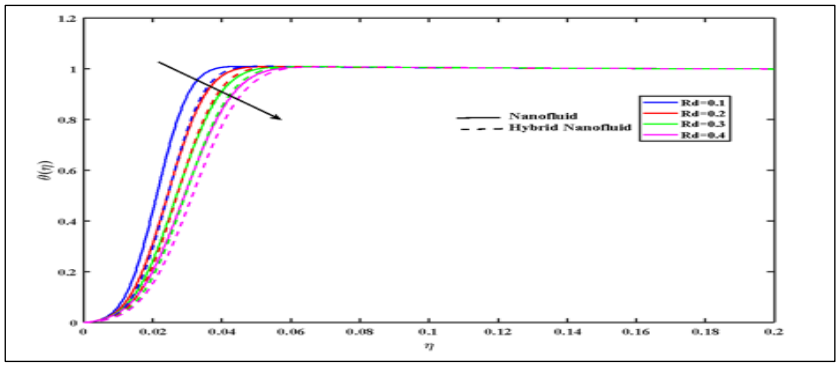

Figure 16: Influence of Thermal Radiation Rd on $\theta(\eta)$

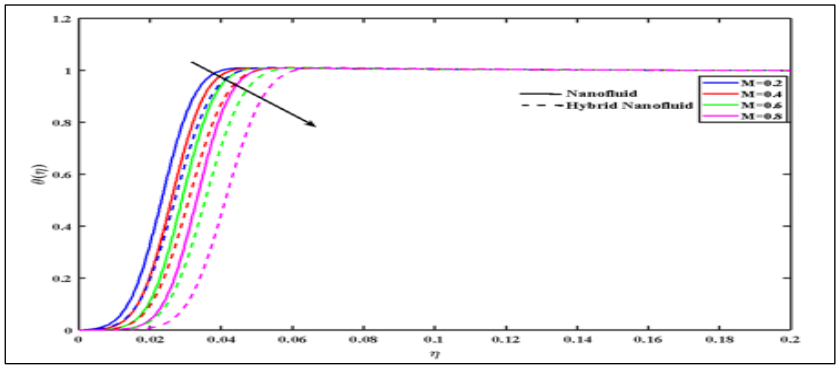

Figure 17: Influence of Melting Parameter m on $\theta(\eta)$

It is analyzed that temperature profile decays with increments in m. Figure 14 reveals the influence of magnetic parameter on the temperature profile, indicating that temperature profile decays with increment in the values of Ha. In Figure 15, the involvement of Ec on $\theta(\eta)$ is presented. Due to the enrichment of Ec, significant improvement has been noticed in the temperature profile. The impact of radiation parameter Rd on temperature profile is shown in Figure 16 It is observed that, $\theta(\eta)$ decreases due to increase in the radiation parameter. Figure 17 reveals the impact of melting parameter on the temperature field. It shows that when M increases, the temperature profile decreases. The physical entrance of cold fluid particles from the melting sheet into a hot fluid is indicated by an increase in M.

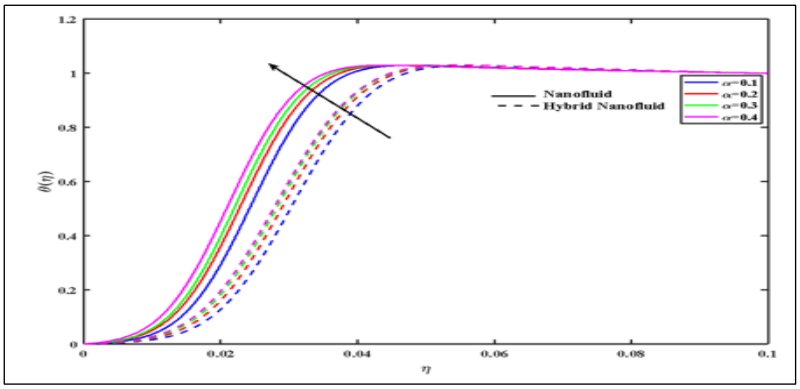

Figure 18: Influence of Wall Thickness α on $\theta(\eta)$

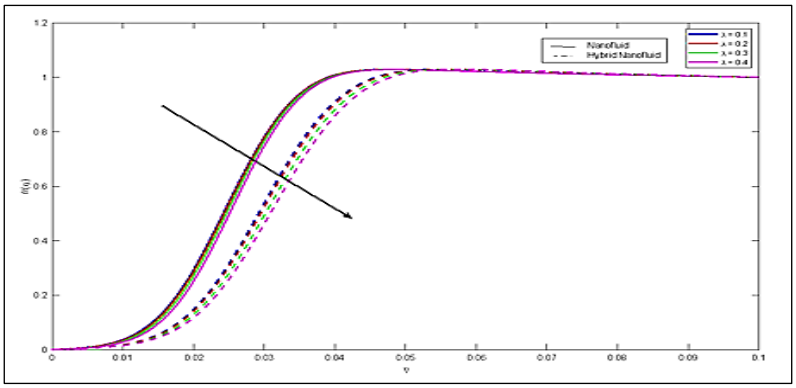

Figure 19: Influence of Hall Effect λ on $\theta(\eta)$

The nature of $\theta(\eta)$ with increases in α is shown in Figure 18. The impact of Hall effect λ on temperature field is shown in Figure 19. It is observed that, $\theta(\eta)$ decreases due to increases in Hall current parameter. For higher values of λ, the interaction between the magnetic field and the hall current becomes dominant, it reduces the resistive effects of the Lorentz force on the temperature field. The temperature profile is significantly improved by increasing wall thickness. A notable increase in hybrid nanofluid as compared to nanofluid is observed in all of the aforementioned Figures 11–19.

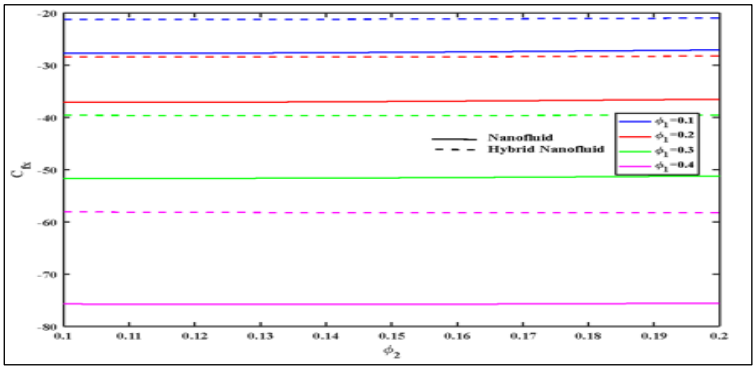

Figure 20: Influence of Skin Friction about φ_1 on φ_2

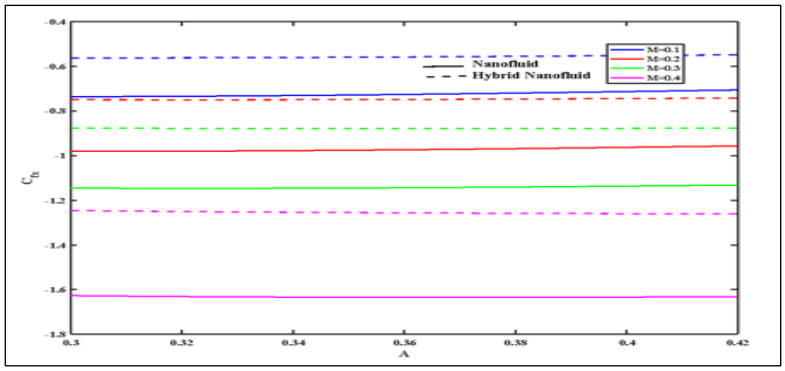

Figure 21: Influence of Skin Friction about M on A

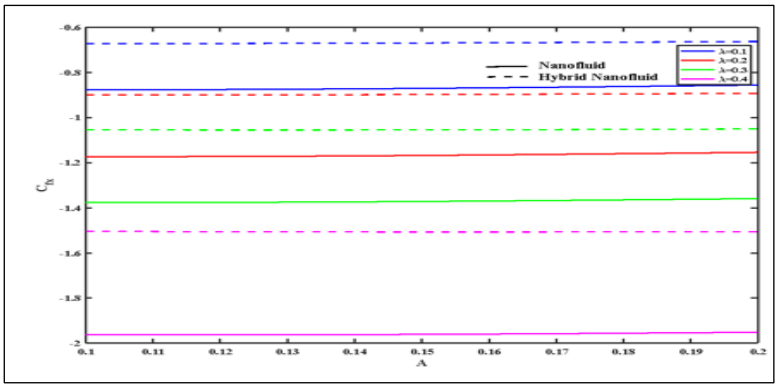

Figure 22: Influence of Skin Friction about λ on A

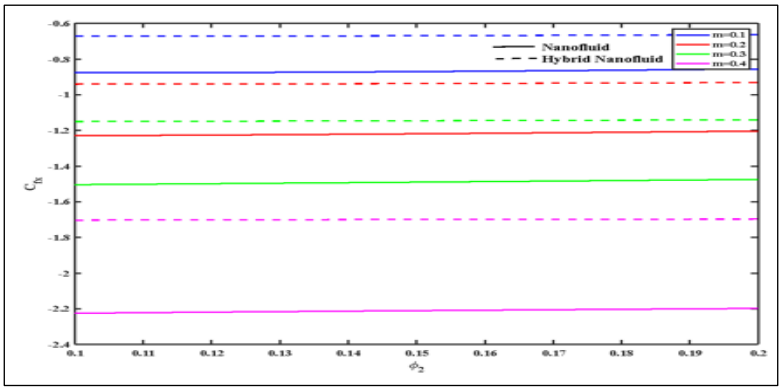

Figure 23: Influence of Skin Friction about M on φ_2

The importance of the skin friction coefficient C_{f_x} as a function of several physical parameters is shown in Figure 20-23. The skin friction coefficient owing to φ_1 is shown graphically in Figure 20. It is found that C_{f_x}decreases with the enhancement of $\varphi_1$as $\varphi_2$grows. The impact of the melting parameter on C_{f_x} is examined in Figure 21. It is evident that C_{f_x}decays with the enrichment of M as the velocity ratio rises. Figure 22 shows how the Hall parameter affects C_{f_x}. It shows that C_{f_x} decreases as the Hall parameter increases as the velocity ratio increases. The impact of the index ratio on $C_{f_x}$is plotted in Figure 23. As the index ratio rises, we can see from the previous figure that C_{f_x}decays.

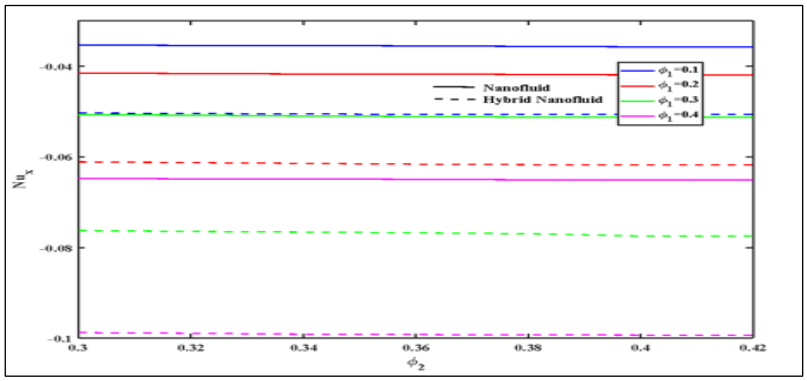

Figure 24: Influence of Nusselt Number about φ_1 on φ_2

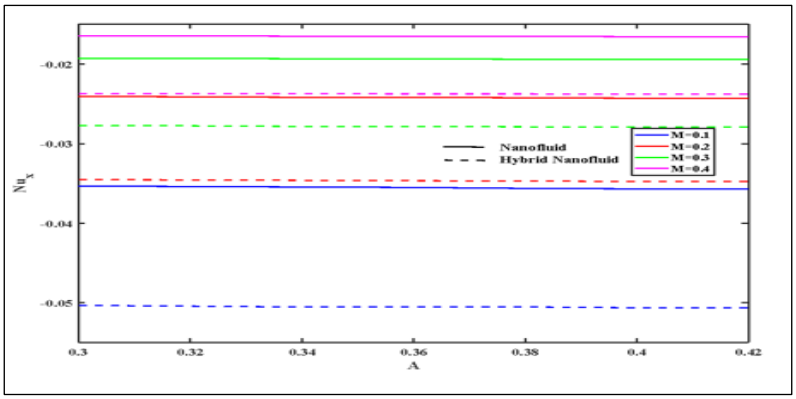

Figure 25: Influence of Nusselt Number about M on A

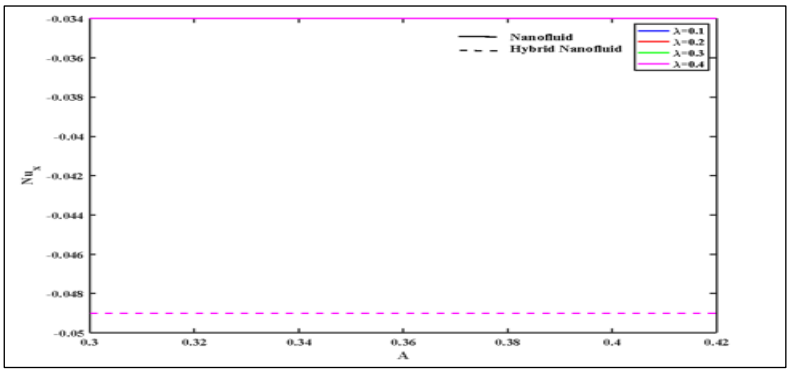

Figure 26: Influence of Nusselt Number about λon A

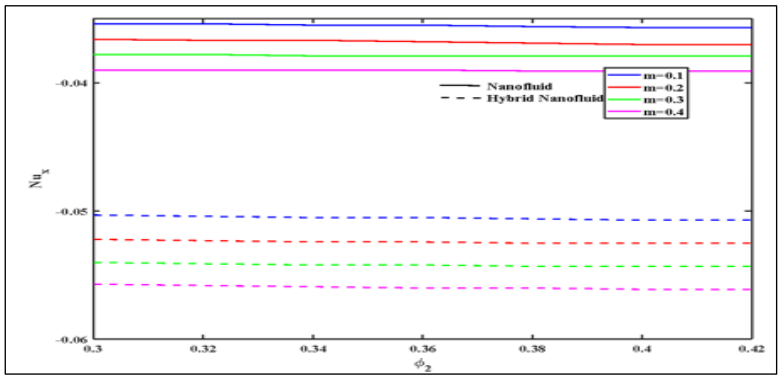

Figure 27: Influence of Nusselt Number about M on φ_2

Figure 24-27 portray the impact of pertinent parameters on local Nusselt number. Figure 24 illustrates Nu_x against φ_1. It has been observed that, as φ_2 increases, Nu_x declines with the enhancement of φ_1. In Figure 25, the influence of melting parameter on Nu_x is studied. It is found that Nu_x intensifies with an increment of M. The significance of Hall parameter on Nu_x is plotted in Figure 26. No significant change is noticed in Nusselt number with the increment of λ. Figure 27 presents the impact of index ratio on local Nusselt number. It shows that for both nanofluids and hybrid nanofluids, the rate of heat transfer decreases with the enhancement of m as $\varphi_2$rises. We can see from the graphs above that hybrid nanofluids behave more efficiently.

Conclusion

The current work is mainly concerned with the effects of Hall effect,thermal radiation, and melting heat on MHD flow of hybrid nanofluid over a variable thickness stretching sheet because of the substantial influence of Hall effect in the engineering area. Core findings of the current research are

- Velocity $f'(\eta)$ maximizes with enhancement in $\varphi_1, \varphi_2, A, M$ and α.

- Velocity profile declines with the enhancement of Ha, m and λ for hybrid nanofluid.
- Temperature (η) is minimized with increme nts in $\varphi_1, \varphi_2, m, Ha, Rd$ and M, reverse behavior is noticed with the enhancement of Ec and α.
- Skin friction lessens with the enhancement in the parameters φ_1, M, λ and m.
- The Nusselt number improves as the melting parameter rises and declines as φ_1, λ and m increases.

The current model may be expanded to other types of hybrid nanofluid and different chemical nanoparticle compositions can be used in the base fluid for the required output. Furthermore, different numerical, analytical and fractional methods can also be used to solve such type of problems.

Abbreviations

u, v: Velocity components, k_f: Thermal conductivit y (gasoline oil), ρ_f: Density (gasoline oil), μ_f: Dynamic viscosity (gasoline oil), α_f: Thermal diffusivity (gasoline oil), υ_f: Kinematic viscosity (gasoline oil), A: velocity ratio parameter, θ: Non-dimensional temperature, m: Behavior index parameter about flow, f: Non-dimensional velocity, q_w: Wall heat flux, T_w: Wall temperature, φ_1: Volume fraction (SWCNTs), φ_2: Volume fraction (Ag), C_s: Heat capacity (solid surface), $(C_p)_f$: Specific heat (gasoline oil), M: Melting parameter, α: Wall thickness parameter, Pr: Prandtl Number, λ: Hall Effect, U_0, U_∞: Arbitrary constant, x, y: Cartesian coordinates,T_∞: Ambient temperature, U_e : Free stream velocity, τ_w : Wall shear stress, U_w: Stretching velocity, β: Latent heat,Ha : Hartmann number, Rd: Radiation, Ec: Eckert number, T_m: Surface temperature, n: Nanoparticle shape parameter, CNTs: Carbon nanotubes, k_{s1}: Thermal conductivity (SWCNTs), k_{s2}: Thermal conductivity (Ag), C_8H_{18} : Gasoline oil, SWCNTs: Single valued carbon nanotubes, Ag: Silver, k_{nf}: Thermal conductivity, $(C_p)_{nf}$: Specific heat, α_{nf}: Thermal diffusivity, ρ_{nf}: Density, μ_{nf} : Dynamic viscosity, υ_{nf}: Kinematic viscosity, k_{hnf} : Thermal conductivi ty, α_{hnf}: Thermal diffusivity, ρ_{hnf}: Densit $(C_p)_{hnf}$: Specific heat, μ_{hnf}: Dynamic viscosity, υ_{hnf}: Kinematic viscosity.

Acknowledgement

None.

Author Contributions

The authors declare that they have contributed equally to this manuscript. Mathematical modelling of the problem, numerical computations and physical interpretations involve rigorous discussions among all the three authors.

Conflict of Interest

The authors state that no conflict of interest exists.

Ethics Approval

Not applicable.

Funding

No funding support was received.

References

1. Choi SUS and Jeffrey Eastman A. Enhancing thermal conductivity of fluids with nanoparticles. Argonne National Lab. (ANL), Argonne, IL (United States).1995. https://www.osti.gov/biblio/196525
2. Vajravelu K. Viscous flow over a nonlinearly stretching sheet. Applied mathematics and computation. 2001 Dec 15;124(3):281-8.
3. Fang T, Zhang J, Zhong Y. Boundary layer flow over a stretching sheet with variable thickness. Appl Math Comput.2012; 218:7241–52.
4. Anjali Devi SP and Prakash M. Thermal radiation effects on hydromagnetic flow over a slandering stretching sheet. Journal of the Brazilian society of mechanical sciences and engineering. 2016;38:423-431.
5. De Volder MF, Tawfick SH, Baughman RH, Hart AJ. Carbon nanotubes: present and future commercial applications. science. 2013 Feb 1;339(6119):535-9.
6. Liu C, Zheng L, Lin P, Pan M, Liu F. Numerical investigation of a two-phase nanofluid model for boundary layer flow past a variable thickness sheet. Zeitschrift für Naturforschung A. 2018 Feb 23;73(3):229-37.
7. Sharma R, Bisht A, Kumar A. Numerical study of fractional boundary layer flow over a stretching sheet with variable thickness: A finite difference approach. InAIP Conference Proceedings. AIP Publishing. 2020 Aug 26;2253(1):020018-28.
8. Roberts L. On the melting of a semi-infinite body of ice placed in a hot stream of air. Journal of Fluid Mechanics. 1958 Sep;4(5):505-28.
9. Gireesha BJ, Mahanthesh B, Shivakumara IS, Eshwarappa KM. Melting heat transfer in boundary layer stagnation-point flow of nanofluid toward a stretching sheet with induced magnetic field. Eng Sci Technol. 2016;19 (1):313–321.
10. Hayat T, Mustafa M, Iqbal Z, Alsaedi A. Stagnation-point flow of couple stress fluid with melting heat transfer. Applied Mathematics and Mechanics. 2013 Feb;34:167-76.
11. Singh K and Kumar M. Melting and heat absorption effects in boundary layer stagnation-point flow

towards a stretching sheet in a micropolar fluid. Ain Shams Engineering Journal. 2018 Dec 1;9(4):861-8.
12. Hayat T, Muhammad K, Farooq, Alsaedi A. Melting heat transfer in stagnation point flow of carbon nanotubes towards variable thickness surface. AIP Adv. 2016; 6:015214(1-2).
13. Turkyilmazoglu M. Natural convective flow of nanofluids past a radiative and impulsive vertical plate. J Aerosp Eng. 2016; 29:1–8.
14. Goud BS, Srilatha P, Bindu P, Krishna YH. Radiation effect on mhd boundary layer flow due to an exponentially stretching sheet. Advances in Mathematics: Scientific Journal. 2020; 9(12):10755–10761.
15. Poply V. Heat transfer in a MHD nanofluid over a stretching sheet. InHeat Transfer-Design, Experimentation and Applications. IntechOpen. 2020 Dec 28;1:1-13.
16. Hayat T and Nadeem S. Heat transfer enhancement with Ag–CuO/water hybrid nanofluid. Results in physics. 2017 Jan 1;7:2317-24.
17. Prasad KV, Vajravelu K, Vaidya H, Van Gorder RA. MHD flow and heat transfer in a nanofluid over a slender elastic sheet with variable thickness. Results in physics. 2017;7:1462-1474.
18. Dey D and Borah R. Numerical simulation of boundary layer flow of MHD influenced nanofluid over an exponentially elongating sheet. In Emerging Technologies in Data Mining and Information Security: Proceedings of IEMIS. Singapore: Springer Nature Singapore. 2022; 1:13-24.
19. Daniel YS, Aziz ZA, Ismail Z, Salah F. Impact of thermal radiation on electrical MHD flow of nanofluid over nonlinear stretching sheet with variable thickness. Alexandria Engineering Journal. 2018 Sep 1;57(3):2187-97.
20. Vajravelu K, Prasad K V, Vaidya H. Influence of Hall Current on MHD Flow and Heat Transfer over a slender stretching sheet in the presence of variable fluid properties. Communications in Numerical Analysis. 2016; 1:17 - 36.
21. Parida SK and Santosh C. MHD viscous nanofluid heat and mass transfer over a nonlinearly stretched sheet: A numerical analysis. Authorea Preprints. 2023 Apr 14. doi:10.22541/au.168146103.38674968/v1
22. Ali A, Khan HS, Noor I, Pasha AA, Irshad K, Al Mesfer MK, Danish M. Hall effects and Cattaneo–Christov heat flux on MHD flow of hybrid nanofluid over a varying thickness stretching surface. Modern Physics Letters B. 2024 Jun 30;38(18):2450130.
23. Muhammad K, Hayat T, Alsaedi A and Asghar S. Stagnation point flow of basefluid (gasoline oil), nanomaterial (CNTs) and hybrid nanomaterial (CNTs+ CuO): a comparative study. Mater Res Express. 2019; 6:105003(1-24).
24. Hayat T, Muhammad K, Farooq M, Alsaedi A. Melting heat transfer in stagnation point flow of carbon nanotubes towards variable thickness surface. AIP Adv. 2016; 6(1):015214.
25. Muhammad K, Hayat T, Alsaedi A. Numerical study for melting heat in dissipative flow of hybrid nanofluid over a variable thicked surface. International Communications in Heat and Mass Transfer. 2021 Feb 1;121:104805.
26. Basit A, Zahid M, Liśkiewicz G. Analysis of MHD hybrid nanofluid through an exponential stretching sheet with dissipation and radiation effects. Authorea Preprints. 2023 Aug 11;6:1-25.